Applied Physics Letters

Understanding and optimization of graphene gas sensors

Cite as: Appl. Phys. Lett. **119**, 013104 (2021); https://doi.org/10.1063/5.0057066
Submitted: 17 May 2021 . Accepted: 15 June 2021 . Published Online: 06 July 2021

Ti Xie, Qin Wang, Robert M. Wallace, and Cheng Gong

AIP Publishing

Applied Physics Letters ARTICLE scitation.org/journal/apl

Understanding and optimization of graphene gas sensors

Cite as: Appl. Phys. Lett. **119**, 013104 (2021); doi: 10.1063/5.0057066
Submitted: 17 May 2021 · Accepted: 15 June 2021 ·
Published Online: 6 July 2021

Ti Xie,[1] Qin Wang,[2] Robert M. Wallace,[3] and Cheng Gong[1,a)]

AFFILIATIONS

[1]Department of Electrical and Computer Engineering and Quantum Technology Center, University of Maryland, College Park, Maryland 20742, USA
[2]Department of Nutrition and Food Science, University of Maryland, College Park, Maryland 20742, USA
[3]Department of Materials Science and Engineering, University of Texas at Dallas, Richardson, Texas 75080, USA

[a)]**Author to whom correspondence should be addressed:** gongc@umd.edu

ABSTRACT

Graphene holds great promise in gas sensor applications due to its excellent electrical transport properties and extraordinarily large surface-to-bulk ratio, rendering the whole atomic-thin films easily affected by gaseous molecules. One unique feature of graphene-based gas sensors is their reversible molecular physical adsorption/desorption mechanism that does not noticeably cause structural distortion or property degradation that chemical reactions would. Given the underlying principle of graphene sensors is the charge transfer between gases and graphene, the initial graphene doping level should be critical in the final sensor performance; however, such knowledge has been largely missed in prior reports. Here, we fabricated graphene transistors to examine the sensor properties using prototypical testing gas NO_2. We found that the distinct initial doping levels of graphene may lead to opposite electrical responses when graphene sensors are exposed to NO_2. The electrical response is triggered by the charge transfer between graphene and NO_2 (and its dimer N_2O_4). Our work highlights the role of graphene conditions in sensor performance, suggests the practical avenues to optimize graphene sensors, and unravels the complex interactions between adsorbed molecules and graphene, which provide valuable guidance for the mass production of commercialized graphene sensors.

Gas sensors have a wide range of potential applications, including chemical plant safeguarding, disease rapid diagnosis, and food spoilage and fruit maturity monitoring. Metal oxide thin films and nanoparticles based devices[1,2] have occupied the significant share of the commercial gas sensor market primarily due to their facile fabrication and excellent detection sensitivity. However, three fundamental factors limit the prospects of metal-oxide-based gas sensors. First, the facile fabrication does not generate high-quality single crystals. Hence, thin films consist of many structural imperfections such as grain boundaries and defects, and nanoparticles cannot be identical in size, geometry, and chemistry. Such factors cause nonuniformity and irreproducibility in device performance. Second, while gaseous molecules approach thin films or packed nanoparticles, penetration and chemical reactions occur, leading to structural distortion and performance degradation. Third, though with large surface-to-bulk ratio, thin films and nanoparticles still hardly reach extreme surface-to-bulk ratio (i.e., 100%).

Since the discovery of graphene, substantial interest has been aroused to develop graphene gas sensors.[3–7] In high-quality single crystalline graphene sheets, the surface-to-bulk ratio reaches 100%, and structural imperfections can be eliminated. Furthermore, when gaseous molecules are adsorbed on graphene, the physical adsorption and ensuing desorption are reversible and this process does not cause structural distortion and property degradation. Once molecules are adsorbed on graphene, there will be electron transfer happening,[3,8–10] and the specific transferring direction depends on the relative energy levels of molecules and graphene. All these characteristics make graphene appealing candidates for next-generation gas sensors.

The general working principle of a graphene sensor is when graphene is originally p-type doped (hole rich), transferring electrons to graphene will reduce graphene's electrical conductivity, while transferring electrons from graphene to molecules will increase graphene's electrical conductivity; when graphene is originally n-type doped (electron rich), the outcomes discussed above will be reversed. As evident, the initial doping level of graphene is critical for the final sensor performance. Specifically, in the commercial domain, mass production of graphene sensors in similar doping levels should be an important prerequisite. However, in laboratory proof-of-concept experiments, this critical factor in the graphene sensor properties has been largely

overlooked, and it has been presumed that graphene is usually p-type doped by polymethyl methacrylate (PMMA) residues, photoresist residues, and/or water.

In this work, we synthesized single-layer graphene on copper foils by chemical vapor deposition (CVD),[11] transferred CVD graphene onto 7 nm-SiO_2/Si chips by PMMA which was removed by chemical solutions afterward (see details in Ref. 12), and fabricated graphene devices by depositing a pair of 5 nm-Ti/70 nm-Au electrodes on a 1 cm-long 4 mm-wide graphene sheet using shadow masks. The as-prepared graphene devices are typically highly p-type doped by PMMA residues, as reported previously.[13]

It has been well known that chemical removal of PMMA still leaves a large amount of PMMA residues, which usually cause high p-type doping in graphene, worsen the metal-graphene contact,[14] and reduce the electron mobility in graphene. More critically, for sensor applications, PMMA residues on the graphene surface may prevent the efficient electron transfer between adsorbed molecules and graphene, resulting in the compromised sensor performance. Therefore, minimizing PMMA residues is an important step to optimize graphene sensors. To this end, we progressively annealed the transferred graphene sample in an ultrahigh vacuum (UHV, $\sim 10^{-10}$ Torr) chamber.

Our home-built UHV system allows the *in situ* annealing in conjunction with Fourier-transform infrared spectroscopy (FTIR). During UHV annealing at progressively elevated temperatures, we monitored the material evolution details by FTIR. Figures 1(b) and 1(c) clearly showed the PMMA decomposition during thermal annealing, evidenced by the reduced amount of CH_2-, CH_3-, and C=O functional groups. Consistent with literature, annealing can strengthen the intimate contact between graphene and the SiO_2/Si chip by removing the trapped water and bubbles at graphene/SiO_2 interfaces,[15] which was

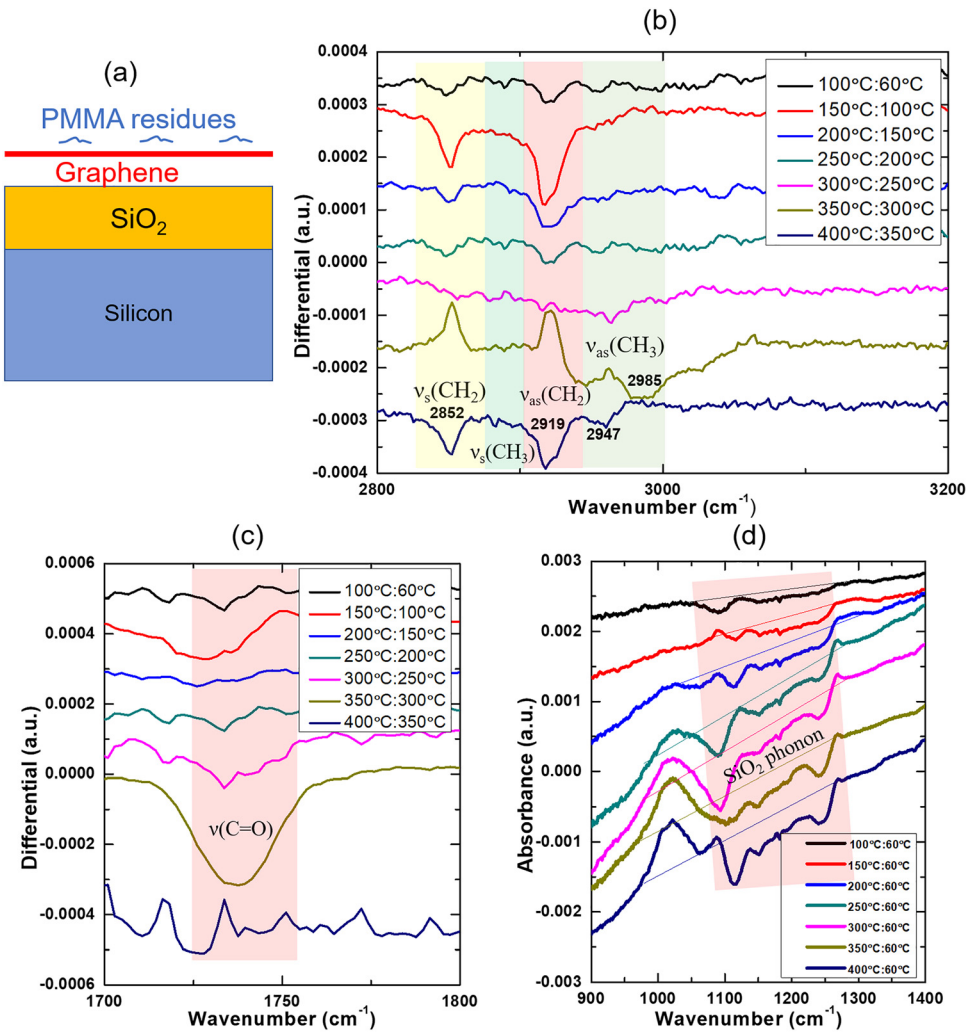

FIG. 1. FTIR characterization of annealed graphene. (a) Side-view illustration of graphene transferred on a SiO_2/Si chip. (b) Differential FTIR spectra of a progressively annealed graphene sample, showing the decomposition of PMMA (i.e., reduction of CH_2- and CH_3- groups). (c) Differential FTIR spectra of the progressively annealed graphene sample, showing the decomposition of PMMA (i.e., reduction of C=O groups). (d) Differential FTIR spectra of the progressively annealed graphene sample, indicating the increasingly intimate graphene-SiO_2 contact which was evidenced by the suppressed SiO_2 phonon absorption.

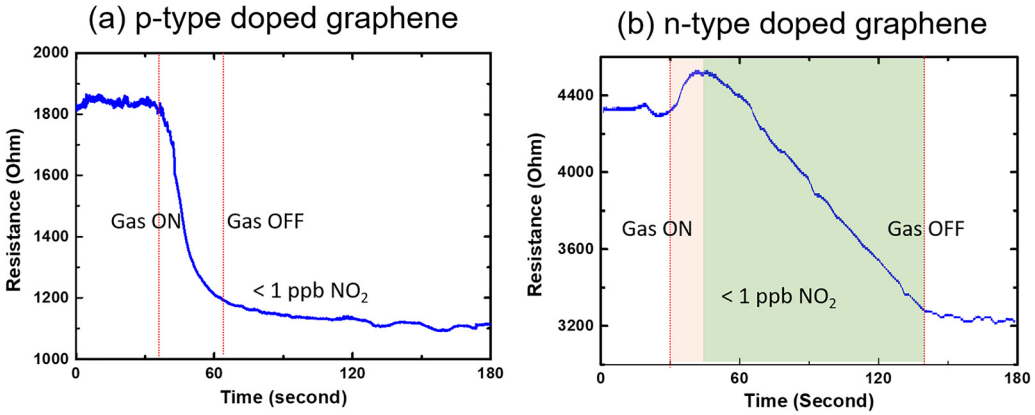

FIG. 2. The electrical characterization of the sensor performance of two different graphene samples for the detection of <1 ppb NO_2. (a) Characterization of p-type graphene as NO_2 sensor. (b) Characterization of n-type graphene as NO_2 sensor. The graphene sample in (a) was prepared with relatively less annealing in UHV (i.e., 200 °C in a UHV chamber of 10^{-10} Torr for 5 h), so the graphene remained p-type doped and its electrical resistance decreases with NO_2 exposure. The graphene sample in (b) was prepared with more extensive annealing in UHV (i.e., 300 °C in a UHV chamber of 10^{-10} Torr overnight, typically about 10 h), so the graphene became n-type doped due to the reduced PMMA residues, the reduced trapped water, and the increased contact with SiO_2 substrate (SiO_2 substrate is one of the n-type doping sources for graphene[16]). The electrical resistance of n-type graphene will increase with NO_2 exposure, and afterward when it is converted to be p-type its electrical resistance will decrease with NO_2 exposure, as shown in (b).

also evidenced by our observation that the increasingly intimate graphene-SiO_2 contact gradually suppressed the SiO_2 phonon absorption [see Fig. 1(d)]. The removal of PMMA residues and trapped water at interface helps recover the transferred graphene toward the intrinsic (i.e., with the least doping).

After annealing graphene in the UHV chamber, we electrically measured the sensor performance by introducing NO_2 into the chamber through a leak valve, while the graphene sensor is kept at liquid nitrogen (LN_2) temperature (after the miniscule introduction of NO_2 the chamber pressure slightly increased to $\sim 10^{-8}$ Torr; equivalent to <1 ppb NO_2). When graphene is mildly annealed (i.e., 200 °C in a UHV chamber of 10^{-10} Torr for 5 h), as shown by Fig. 2(a), upon the introduction of NO_2, the electrical resistance of the graphene device immediately drops. As expected, NO_2 dopes graphene by holes and increases the electrical conductivity of the originally p-type graphene.

Given that the graphene sensor was kept at LN_2 temperature, the adsorbed NO_2 was "frozen" on the sensor: that is, after turning off the NO_2 supply, the adsorbed NO_2 molecules remained on the sensor and the sensor electrical resistance did not reverse back to the original value. We intentionally designed the LN_2-temperature adsorption experiments so that FTIR can be applied to study the detailed sensor mechanism—i.e., how NO_2 is adsorbed on graphene. Without LN_2-temperature function, the adsorbed NO_2 would immediately desorb and the detailed molecular adsorption configuration would not be experimentally captured.

Remarkably, for another graphene sample with more extensive annealing treatment (i.e., 300 °C in a UHV chamber of 10^{-10} Torr overnight, typically about 10 h), as shown in Fig. 1(b), the electrical resistance increases at first and then decreases. This behavior was reproducible. It clearly indicated that the extensive vacuum annealing

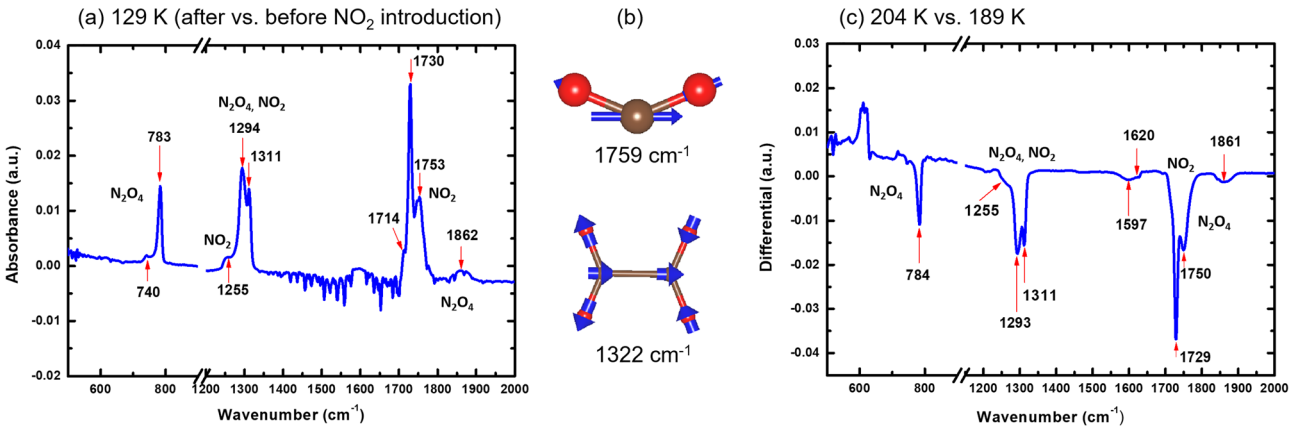

FIG. 3. FTIR absorption spectra of NO_2 on graphene and the calculated vibrational frequencies of NO_2 and N_2O_4 molecules. (a) FTIR absorption spectra of NO_2 on graphene. (b) Calculated representative vibrational frequencies of NO_2 and N_2O_4 molecules. (c) FTIR differential spectra of NO_2 on graphene on 204 K vs 189 K.

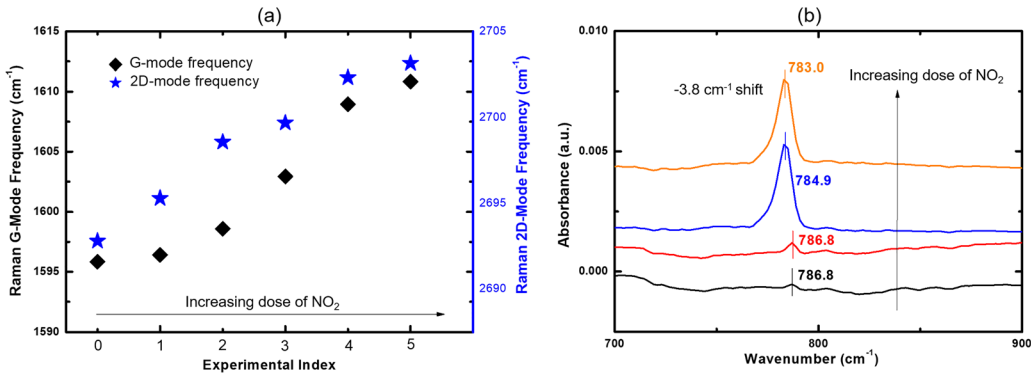

FIG. 4. Vibrational frequencies of NO_2-graphene complex as a dependence on NO_2 dose at 77 K. (a) Raman G-peak and 2D-peak of graphene as a dependence on the NO_2 dose. (b) Infrared absorption spectra of NO_2-graphene as a dependence on the NO_2 dose.

makes graphene slightly n-type doped. This is consistent with prior reports that the clean SiO_2 surface tends to n-type dope graphene.[16] After extensive annealing, the n-type doping of graphene caused by SiO_2 outperforms the p-type doping of graphene caused by PMMA residues and trapped water. Once graphene becomes n-type doped, the NO_2 introduction (providing holes) will compensate the electrons in graphene and cause the increased electrical resistance. After full compensation, graphene is converted into p-type, when its resistance would keep decreasing with NO_2 exposure. Our results revealed the significant role of the original graphene doping level in the final sensor performance.

To understand the sensor mechanism from the atomic/molecular scale, we used the low temperature to "freeze" the adsorbed NO_2 on graphene and then conducted the FTIR study to analyze the adsorption molecular details. Obvious NO_2 features were revealed in the FTIR absorption spectrum at a low temperature of 129 K [see Fig. 3(a)]. Then, we gradually increased the temperature to release NO_2 to desorb from graphene. As expected, the adsorbed NO_2 gradually left graphene at elevated temperature [see Fig. 3(c)]. The interesting observation here is that many absorption features are not from individual NO_2 molecules but from the dimer N_2O_4. The assignment of these peaks to NO_2 or N_2O_4 is based on reference to literature[17] and our density functional theory (DFT) calculation[18–20] of the molecular vibrational frequencies [see Fig. 3(b)]. It is obvious that the adsorbed NO_2 molecules have mutual interactions between neighboring molecules, rather than only being separately adsorbed.

In DFT calculations, the NO_2 and N_2O_4 molecules are modeled in a super cell with 15 Å vacuum gaps along x-, y-, and z-directions to minimize the interaction between adjacent images. The calculations are performed using Vienna *Ab initio* Simulation Package (VASP)[18] with projector-augmented wave (PAW) pseudopotential[19] with the generalized gradient approximation (GGA) of Perdew–Burke–Ernzerhof (PBE) functional[20] to describe the exchange correlation. Spin polarization is included for gaining the accurate total energies. The ionic relaxation stops when the remnant force on each atom below 0.01 eV/Å. The energy cutoff is chosen at 400 eV, and the electronic optimization stops when the total energies of neighboring optimization loops differ below 10^{-4} eV. The Monkhorst-Pack k-point sampling in Brillouin zone is Γ-centered with $4 \times 4 \times 4$ in electronic optimization. The calculation of the Γ-point vibration frequency is also done by VASP with PBE functional.

Once being adsorbed, the adsorbates and graphene mutually affect each other. As discussed above, NO_2 tends to p-type dope graphene. Indeed, we observed a monotonic increase in graphene's Raman G-mode frequency with the increasing dose of NO_2, as shown in Fig. 4(a). It has been well known that graphene's G-peak frequency monotonically increases with the doping concentration on both p-type and n-type branches, and graphene's 2D-peak frequency monotonically increases with reduced n-type doping and increased p-type doping.[21] Therefore, our observed monotonic increase in both G-peak and 2D-peak frequencies clearly shows the increasing p-type doping in graphene caused by the progressive NO_2 adsorption.

When graphene's doping level is increased with NO_2 adsorption, we simultaneously observed the N_2O_4 vibrational frequency has a monotonic red shift by 3.8 cm^{-1} [see Fig. 4(b)]. We attribute this red shift of N_2O_4 molecular vibration frequency to the enhanced metallicity of doped graphene that gives rise to the enhanced screening effect, which potentially weakens the intra-molecular bonding of adsorbed N_2O_4. In short, the vibrational frequencies of both graphene and the adsorbates (i.e., NO_2/N_2O_4) were observed to evolve with the NO_2 dose, which clearly tells the mutual effects between adsorbed molecules and graphene.

In summary, we experimentally observed <1 ppb NO_2 detection sensitivity based on centimeter-scale graphene two-terminal electrical devices. The physical adsorption/desorption of NO_2 is reversible without causing noticeable structural distortion or property degradation in graphene. The initial graphene doping level was found to be critical in the gas sensor performance, as highlighted by the opposite electrical responses of the n-type and p-type graphene devices in response to NO_2 exposure. Furthermore, we found that the resultant adsorbates are not merely individual NO_2 molecules but also the dimer N_2O_4. Our work reveals in detail how processing (e.g., vacuum annealing) affects graphene conditions and, finally, the sensor performance. In order to industrialize the mass production of graphene sensors with optimized and reproducible performance, careful measures should be taken to maintain the graphene quality/condition consistency.

R.M.W. acknowledges the support of the Erik Jonsson Distinguished Chair. C.G. acknowledges the support from the startup grant from the University of Maryland, College Park, and the support from Northrop Grumman Mission Systems' University

Research Program. C.G. also acknowledges the fruitful discussions with Yves J. Chabal.

DATA AVAILABILITY

The data that support the findings of this study are available from the corresponding author upon reasonable request.

REFERENCES

[1]C. Wang, L. Yin, L. Zhang, D. Xiang, and R. Gao, Sensors **10**, 2088–2106 (2010).
[2]R. Malik, V. K. Tomer, Y. K. Mishra, and L. Lin, Appl. Phys. Rev. **7**, 021301 (2020).
[3]F. Schedin, A. K. Geim, S. V. Morozov, E. W. Hill, P. Blake, M. I. Katsnelson, and K. S. Novoselov, Nat. Mater. **6**, 652–655 (2007).
[4]H. J. Yoon, D. H. Jun, J. H. Yang, Z. Zhou, S. S. Yang, and M. M.-C. Cheng, Sens. Actuators, B **157**, 310–313 (2011).
[5]W. Yuan and G. Shi, J. Mater. Chem. A **1**, 10078–10091 (2013).
[6]M. G. Chung, D. H. Kim, H. M. Lee, T. Kim, J. H. Choi, D. K. Seo, J.-B. Yoo, S.-H. Hong, T. J. Kang, and Y. H. Kim, Sens. Actuators, B **166–167**, 172–176 (2012).
[7]A. Nag, A. Mitra, and S. C. Mukhopadhyay, Sens. Actuator, A **270**, 177–194 (2018).
[8]J. Kong, N. Franklin, C. Zhou, M. Chapline, S. Peng, K. Cho, and H. Dai, Science **287**, 622–625 (2000).
[9]S. Peng, K. Cho, P. Qi, and H. Dai, Chem. Phys. Lett. **387**, 271–276 (2004).
[10]A. Azizi, M. Dogan, H. Long, J. D. Cain, K. Lee, R. Eskandari, A. Varieschi, E. C. Glazer, M. L. Cohen, and A. Zettl, Nano Lett. **20**, 6120–6127 (2020).
[11]X. Li, W. Cai, J. An, S. Kim, J. Nah, D. Yang, R. Piner, A. Velamakanni, I. Jung, E. Tutuc, S. K. Banerjee, L. Colombo, and R. S. Ruoff, Science **324**, 1312–1314 (2009).
[12]C. Gong, H. C. Floresca, D. Hinojos, S. McDonnell, X. Qin, Y. Hao, S. Jandhyala, G. Mordi, J. Kim, L. Colombo, R. S. Ruoff, M. Kim, K. Cho, R. M. Wallace, and Y. J. Chabal, J. Phys. Chem. C **117**, 23000–23008 (2013).
[13]A. Pirkle, J. Chan, A. Venugopal, D. Hinojos, C. W. Magnuson, S. McDonnell, L. Colombo, E. M. Vogel, R. S. Ruoff, and R. M. Wallace, Appl. Phys. Lett. **99**, 122108 (2011).
[14]J. A. Robinson, M. LaBella, M. Zhu, M. Hollander, R. Kasarda, Z. Hughes, K. Trumbull, R. Cavalero, and D. Snyder, Appl. Phys. Lett. **98**, 053103 (2011).
[15]Z. Cheng, Q. Zhou, C. Wang, Q. Li, C. Wang, and Y. Fang, Nano Lett. **11**, 767–771 (2011).
[16]H. E. Romero, N. Shen, P. Joshi, H. R. Gutierrez, S. A. Tadigadapa, J. O. Sofo, and P. C. Eklund, ACS Nano **2**, 2037–2044 (2008).
[17]L. Harris, W. S. Benedict, and G. W. King, Nature **131**, 621 (1933).
[18]G. Kresse and J. Furthmuller, Comput. Mater. Sci. **6**, 15–50 (1996).
[19]P. E. Blochl, Phys. Rev. B **50**, 17953–17979 (1994).
[20]J. P. Perdew, K. Burke, and M. Ernzerhof, Phys. Rev. Lett. **77**, 3865 (1996).
[21]A. Das, S. Pisana, B. Chakraborty, S. Piscanec, S. K. Saha, U. V. Waghmare, K. S. Novoselov, H. R. Krishnamurthy, A. K. Geim, A. C. Ferrari, and A. K. Sood, Nat. Nanotechnol. **3**, 210–215 (2008).